INORGANIC CHEMISTRY FRONTIERS

RESEARCH ARTICLE

View Article Online
View Journal | View Issue

Cite this: *Inorg. Chem. Front.*, 2023, **10**, 2438

A dense 3d–4f metal–organic framework with "gas pockets" for highly efficient CH_4/N_2 separation†

Li-Min Zhu,[a] Wen-Liang Li,[a] Tian-Ran Li,[a] Lin-Ping Shi,[a] Li-Ting Li,[a] Zhao-Quan Yao,*[a] Hong-Liang Huang, *[b] Jiong-Peng Zhao *[a] and Fu-Chen Liu *[a]

In this work, we report a multi-component MOF $[CuCe\ L(Cl_4\text{-}bdc)_{0.5}(H_2O)_2{\cdot}(H_2O)_6]_n$ (L = 1*H*-pyrazole-3,4,5-tricarboxylic acid, Cl_4-bdc = 2,3,5,6-tetrachloroterephthalate) with a pillar-layered structure. In the structure, the polydentate ligand (L) linked Cu^{II} and Ce^{III} atoms constitute 3d–4f layers that serve as the pedestal base and the chlorinated Cl_4-bdc ligands acting as bolsters are installed between the layers through Ce^{III}. The moderate pore size and the unique chloride decorated surface of channels endow this MOF with excellent separation ability for methane (CH_4) and nitrogen (N_2). According to the adsorption tests, this MOF exhibits a high adsorption capacity for CH_4 (28.41 cm^3/cm^3) at 298 K and 1 bar, while the N_2 adsorption capacity is only 3.43 cm^3/cm^3. The DFT calculations demonstrate that the adjacent Cl_4-bdc in the network can act as "gas pockets" or nano traps to immobilize the CH_4 molecules effectively through multiple interactions between Cl atoms and CH_4. The high performance of this MOF in CH_4/N_2 separation has been verified by the outstanding IAST selectivity of 13.32 and breakthrough experiments. This work provides a new perspective for capturing CH_4 from coal-mine gas to recover fuel and reduce greenhouse gas emissions.

Received 7th February 2023,
Accepted 15th March 2023

DOI: 10.1039/d3qi00235g

rsc.li/frontiers-inorganic

Due to the rapid consumption of fossil fuels, energy and environmental problems have to be solved urgently in this century. Conventional natural gas (mainly composed of methane) is considered to be an ideal alternative to petroleum fuels because of its abundance and cleanliness.[1] Unconventional natural gas (such as coal bed methane (CBM), landfill gas, and shale gas) also produces a large amount of methane, which is an excellent complement to conventional natural gas.[2] Currently, due to the lack of suitable purification methods, a large amount of methane is introduced into air, which not only brings about a serious greenhouse effect (21 times that from CO_2) but also causes a waste of energy.[3] Therefore, utilization of this low-quality natural gas is extremely important. Generally, in unconventional natural gas, the concentration of nitrogen (N_2) is much higher than that of methane (*e.g.* the methane concentration in CBM is less than 30%), which limits its direct utilization.[2,3] So, the separation of CH_4/N_2 mixtures to obtain high purity methane has important industrial value. Currently, the prevalent industrial approach to separate methane from CH_4/N_2 mixtures is cryogenic distillation (boiling point: 112 K for CH_4 and 77 K for N_2) which is not only an energy-intensive process but also a burden to the environment.[4] Thus, a cost- and energy-efficient CH_4/N_2 separation process is urgently desired.

Compared with traditional cryogenic distillation methods, adsorbent-based gas adsorption using porous materials is an economical and energy-efficient method.[5] Many traditional porous materials, such as zeolites and porous carbons, have been extensively studied for CH_4 purification.[6–12] Although these kinds of porous material adsorbents have been widely reported and have exhibited prominent adsorption separation performance toward CH_4/N_2 mixtures, their selectivity and yields are still low. The main reason is the similar physical properties of CH_4 and N_2, including polarizability and kinetic diameters (3.8 Å for CH_4 and 3.64 Å for N_2).[13–23] As a new class of crystalline porous materials, metal–organic frameworks (MOFs) featuring diverse structures, programmable topology, and tailorable and modifiable porosity offer an ideal platform for gas adsorption and separation.[3,24–26] Besides, the crystal-

[a]*School of Chemistry and Chemical Engineering, TKL of Organic Solar Cells and Photochemical Conversion, Tianjin University of Technology, Tianjin 300384, China. E-mail: yaozq@email.tjut.edu.cn, zhaojp@tjut.edu.cn, fcliu@tjut.edu.cn*
[b]*School of Chemistry and Chemical Engineering, Tiangong University, Tianjin 300387, China. E-mail: huanghongliang@tiangong.edu.cn*

†Electronic supplementary information (ESI) available: Additional crystallographic data. CCDC 2223795. For ESI and crystallographic data in CIF or other electronic format see DOI: https://doi.org/10.1039/d3qi00235g

line nature of MOFs also provides an opportunity to investigate the gas adsorption mechanisms. Up to now, various methods have been used to improve the separation performance of CH_4/N_2 in MOF systems including the design and synthesis of new structures, decorating with functional groups, compositing with other materials *etc*. By using these methods, although the interaction between CH_4 and frameworks has been improved, the adsorption and separation performances are still unsatisfactory.[18,20,27,28] Inspired by the vital effect of R–H···X (X = heteroatoms in MOFs) interaction in hydrocarbon (alkene and alkane, alkene and alkyne) separation,[29–34] decorating heteroatoms in the inner wall of channels or frameworks might endow the frameworks with a stronger binding effect for CH_4. Besides, considering the non-polar nature of CH_4 molecules, anchoring heteroatoms to specific sites (*e.g.* cages or nanopores) using the inherent confinement effect to enhance the host framework–guest CH_4 molecule interaction might be a promising protocol (Scheme 1).

In this work, a novel pillar-layered MOF $[CuCeL(Cl_4\text{-}bdc)_{0.5}(H_2O)_2\ (H_2O)_6]_n$ (**1**) (L: 3,4,5-pyrazoletricarboxylate; Cl_4-bdc: 2,3,5,6-tetrachloroterephthalate) has been constructed successfully. In this structure, L connected Ce^{III} and Cu^{II} atoms form 3d–4f layers, while the Cl_4-bdc ligands which act as pillars are installed between layers through Ce^{III} to form the 3D-pillar-layered framework with obvious 1D channels (9.0 Å × 9.5 Å) along the *a*-axis. On the sides of the channels, a large number of small hallways constructed by the adjacent Cl_4-bdc ligands were formed (5.0 Å × 7.0 Å × 9.5 Å). According to the result of DFT calculation, due to the synergistic effect between the confinement effect and abundant C–H···Cl interactions in these small hallways, the methane molecules can be trapped in these confined spaces effectively. As a result, **1** presents a high adsorption capacity for CH_4 (28.41 cm^3/cm^3 at 298 K) and a high IAST selectivity of 13.32 for CH_4/N_2 separation.

Single-crystal X-ray diffraction study on a suitable single crystal of $[CuCeL(Cl_4\text{-}bdc)_{0.5}(H_2O)_2\cdot(H_2O)_6]_n$ at 298 K revealed that **1** crystallizes in the triclinic space group $P\bar{1}$ (Table S1†) with high densities of 2.145 g cm^{-3} and 1.700 g cm^{-3} for the complex and the activated framework, respectively. The asymmetric unit cell has one Ce^{III}, one Cu^{II}, one L ligand, half Cl_4-bdc ligand, two coordinated water molecules and six free water molecules (Fig. S1†). As shown in Fig. 1a, each Cu ion presents

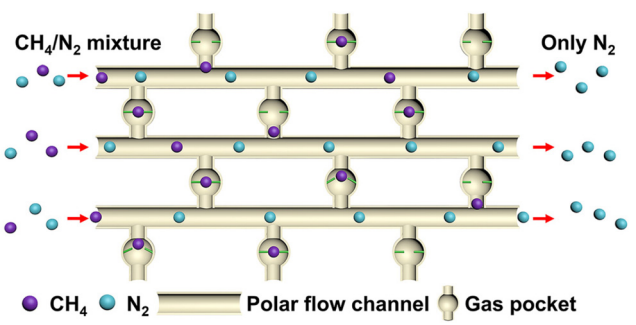

Scheme 1 Schematic representation of the 1D channels and gas pockets in this pillar-layered MOF.

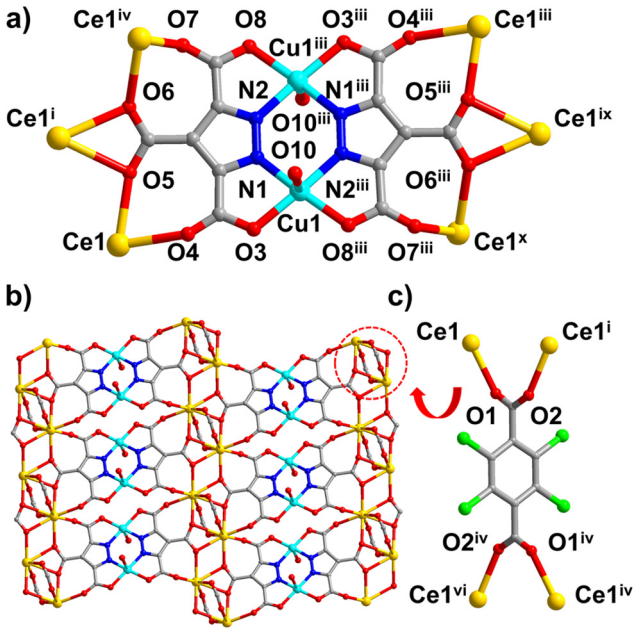

Fig. 1 (a) Coordination modes and linkage of the Cu ions and L ligands. (b) The 3d–4f Cu–Ce layer bridged by L ligands. (c) Coordination modes of bridging Cl_4-bdc ligands. Symmetry codes: [i] 2 − *X*, 1 − *Y*, 1 − *Z*; [ii] 1 + *X*, +*Y*, +*Z*; [iii] 1 − *X*, 1 − *Y*, −*Z*; [iv] −1 + *X*, +*Y*, +*Z*; [v] 2 − *X*, 2 − *Y*, 1 − *Z*; [vi] +*X*, 1 + *Y*, +*Z*; [vii] 3 − *X*, 1 − *Y*, 1 − *Z*; [viii] 2 + *X*, +*Y*, +*Z*; [ix] −1 + *X*, +*Y*, −1 + *Z*; [x] 2 − *X*, 1 − *Y*, −*Z*.

a pyramidal coordination geometry: two Cu1 are chelated by two L ligands to form a $Cu_2N_4O_4$ coordination plane, in which N1, O3, and $N2^{iii}$, $O8^{iii}$ are assigned to two L ligands, respectively. The axial positions of each Cu ion are occupied by one water molecule (O10). In this manner, two Cu ions (Cu1 and $Cu1^{iii}$) are bridged by two L ligands forming a Cu_2L_2 plane (Fig. 1a, Table S2†). The residual carboxyl oxygen atoms in L are coordinated to six Ce ions in the chelating mode to form the 3d–4f Cu–Ce layer (Fig. 1b). In this layer structure, each Ce^{III} ion is coordinated with five oxygen atoms which can be assigned to three L ligands (O4, O5, O6, O7) and a water molecule (O9), respectively. However in the perpendicular direction of the layer, each Ce^{III} ion is coordinated with four oxygen atoms which come from two Cl_4-bdc ligands (O1 and O2) (Fig. 1c and S2†). Consequently, the Cl_4-bdc ligands serve as pillars to sustain the neighbouring 3d–4f layers into a 3D framework with 1D open channels along the *a* and *c* axes (Fig. 2a–c).

As shown in Fig. 2a, the framework of **1** has moderate 1D channels with a rectangular cross-section in dimensions of 9.0 × 9.5 Å along the *a*-axis. The chlorinated Cl_4-bdc ligands which serve as pillars are located on either side of the channels and provide a large number of chloride atoms on the inner wall of channels. Besides, between the two neighbouring Cu^{II}–Ce^{III} layers, the adjacent Cl_4-bdc ligands also form small cavities or confined spaces in dimensions of 9.5 × 7.0 × 5.8 Å which are vertically distributed on both sides of the one-dimensional channel (Fig. 2c). Due to the narrow size of these cavities and abundant chlorine binding sites, various gas molecules with a

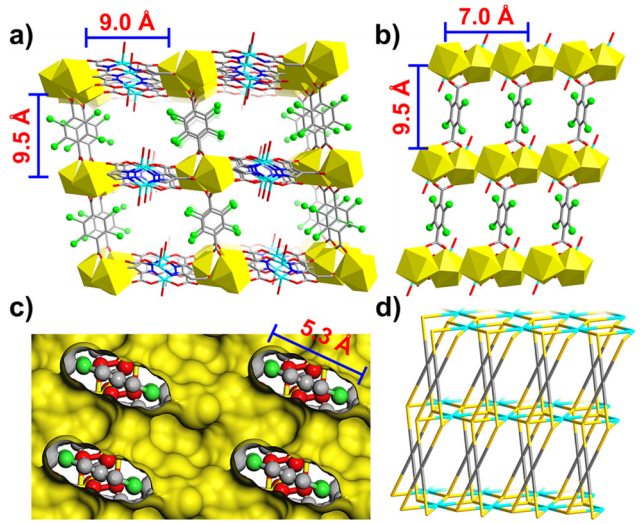

Fig. 2 (a and b) Three-dimensional structural diagram of **1** along the *a* and *c*-axes. Note: in order to clearly express the pore structure, all free solvent (water) molecules are deleted. (c) Internal structure of pores in **1** illustrated using the Connolly surface in yellow along the *b*-axis. (d) The topological map of **1** along the *c*-axis.

small size could access the cavity and be trapped within these "gas pockets". In addition, PLATON analysis shows that the effective free volume of **1** can reach up to 43.3% of the crystal volume after squeezing out free water molecules.[35] To further investigate the structure, the topological simplification of the structure was carried out. As shown in Fig. 2d, the Cu_2L_2 units which connected to six Ce^{III} ions can be viewed as six connected nodes, while the Cl_4-bdc ligands which coordinated with four Ce^{III} ions can be viewed as four-connected nodes. The Ce^{III} ions could be viewed as five-connected nodes. Finally, the whole framework can be simplified as a 4,5,6-connected topological network using the Schläfli notation $\{4^2;8^4\}^{20}\{4^8;6^2\}_2\{4^6;6^6;8^3\}$.[36–38]

Due to the moderate pore size, large porosity, and exposed halogen atoms in specific cavities, this MOF may have a special interaction with some gas molecules and is beneficial in the field of adsorption and separation. Before the adsorption investigation, the purity of **1** and the rigidity of the framework were verified by PXRD and IR under different conditions (Fig. 3a and Fig. S3†). The PXRD data reveal that all diffraction peaks in the experimental patterns match well with the simulation, suggesting the high purity of the synthesized sample. Furthermore, the PXRD patterns of the samples which were immersed in H_2O, acetonitrile, and DMF solutions for 24 hours are also consistent with those obtained by simulation. Even for the sample activated at 146 °C for 8 h, both the PXRD pattern and FT-IR spectra matched well with those of the pristine sample which indicates that **1** could keep the framework intact under these conditions (Fig. 3a and S3†). The thermogravimetric analysis (TGA) of this MOF reveals an obvious weight loss of 20% when the temperature was increased to 152 °C, corresponding to the loss of coordinated and free water molecules in channels (calculated to be 20.7%) and the framework did not collapse until 320 °C, which suggested the good thermal stability of the MOF. The TGA curve of the activated sample showed that almost all water molecules had been removed under the activation process. And the slight mass loss at a low temperature indicated there were still some residues in the channel, which may be attributed to the adsorption of water or VOCs in the air of the activated sample during the sample transfer process.[39] Besides, the framework remained intact until 320 °C, which further proves the excellent stability and rigidity of the framework.

Due to the smaller molecular radius and the better packing ability on the inner surface of Ar than those of diatomic N_2 molecules, the 87 K Ar adsorption measurement was carried out for investigating the permanent porosity of **1**. As shown in Fig. 4a, **1** exhibits a reversible type-I isotherm with the characteristic of microporosity, and the Brunauer–Emmett–Teller (BET) surface area was estimated to be 536.63 $m^2\ g^{-1}$. The experimental total pore volume was determined to be 0.214 $cm^3\ g^{-1}$ (calculated by the single point method at P/P_0 = 0.98). Using nonlocal density functional theory, the pore size distribution was calculated to be 5.4 Å, which is consistent with the value from SCXRD data. Owing to the microporous nature and the unique chlorinated "gas pocket" structure, the

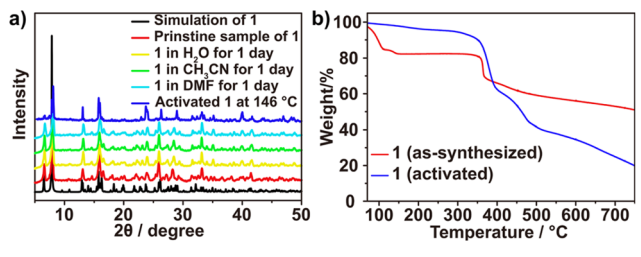

Fig. 3 (a) Powder X-ray diffraction patterns of **1** under different conditions. (b) TGA curves of **1** before and after activation.

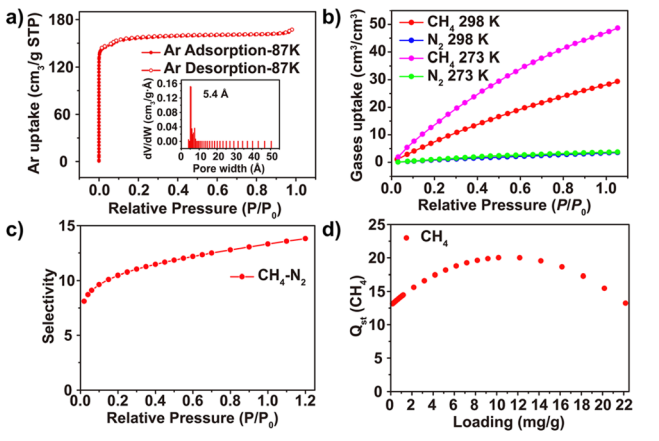

Fig. 4 (a) Ar adsorption/desorption isotherms of **1** at 87 K, inset figure: the pore size distribution of **1**. (b) The CH_4 and N_2 volume adsorption isotherms of **1** at 273 K and 298 K, respectively. (c) IAST selectivity for CH_4/N_2 of the MOF. (d) Q_{st} curves of **1** for CH_4 and N_2.

adsorption capacity for CH_4 gas of **1** was tested at 273 and 298 K, respectively. As shown in Fig. 4b and Fig. S4,† the CH_4 absorption at 273 K and 298 K can reach up to 47.36 cm^3/cm^3 and 28.41 cm^3/cm^3, respectively. However under the same conditions, the adsorption capacities for N_2 are only 3.67 cm^3/cm^3 (273 K) and 3.43 cm^3/cm^3 (298 K). The isosteric enthalpies of adsorption (Q_{st}) of this MOF for CH_4 were calculated from the virial equation based on the isotherms collected at 273 and 298 K. As shown in Fig. 4d, the initial Q_{st} value for CH_4 of **1** is 13.2 kJ mol^{-1}. Besides, with the increase of adsorption capacity, the Q_{st} values for CH_4 exhibit a turnover behaviour.

For an industrial process the volume adsorption capacity is more important than the mass adsorption capacity, and the volume adsorption capacity for CH_4 is a key metric for evaluating the separation effect. As shown in Fig. 5, the adsorption capacity of **1** (28.41 cm^3/cm^3) exceeds that of $Co_3(C_4O_4)_2(OH)_2$ (19.81 cm^3/cm^3), ROD-8 (21.89 cm^3/cm^3), and Ni $(OAc)_2L$ (20.92 cm^3/cm^3) and is comparable to that of $Cu(NIA)_2$, MOF-890 and MOF-889 (Table S3†) but is smaller than that of MOF-891, Al-CDC and ACT-Cu.[14,40,41] In order to verify the separation ability of **1** for CH_4/N_2 separation, the ideal adsorption solution theory (IAST) was used to investigate its CH_4/N_2 selectivity. After calculation and fitting, the IAST selectivity of **1** is shown in Fig. 4c, which indicates a gradually increasing trend in the whole pressure range, and the maximum selectivity at normal pressure is 13.32, which is rare in published MOFs and higher than that of $Co_3(C_4O_4)_2(OH)_2$ (12.5), STAM-1 (11.1) and Al-CDC (13.1) in the first echelon (detailed information can be found in the ESI (Table S3†)).

In addition, DFT calculations were used to investigate the interactions between the MOF and CH_4 molecules. As shown in Fig. 6, multiple interactions occurred between CH_4 and adjacent Cl_4-bdc with a binding energy of CH_4 of −13.95 kJ mol^{-1}, and the distances between the hydrogen atoms of CH_4 and the Cl atoms in Cl_4-bdc ranged from 3.154 to 4.359 Å,

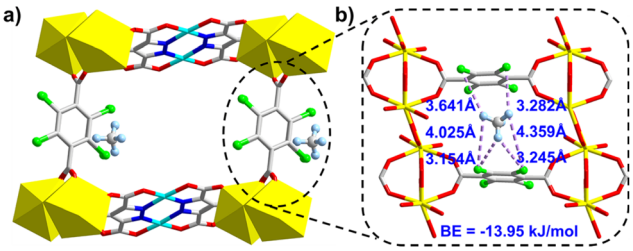

Fig. 6 (a and b) Preferential adsorption sites and binding energies of CH_4 in the MOF obtained from the DFT-optimized structural model; BE stands for binding energy in (b).

which is in the range of the van der Waals' (vdW) interaction. Besides, the adjacent Cl_4-bdc ligands can form confined spaces which not only exhibit multipoint vdW interactions between CH_4 and the host framework but also enhance the interaction by the confinement effect. DFT calculations show that the surface C–Cl plays an important role in the enhancement of the adsorption selectivity of the MOF toward CH_4/N_2 mixtures.

Static adsorption and selectivity calculation indicated that **1** has great advantages in the separation of CH_4/N_2. To further confirm the separation performance of **1** for mixed gases in practical applications, two consecutive cycles of breakthrough experiments of **1** for a CH_4/N_2 (50/50, v/v) mixture were carried out. As shown in Fig. 7, the adsorption time of CH_4 was longer than that of N_2 during the process. N_2 first broke through the packed column, whereas CH_4 was preferentially adsorbed by **1** and broke through the column after a longer time delay which means that a clear separation between CH_4 and N_2 was achieved. Besides, during these two consecutive cycles of breakthrough experiments, the separation ability of **1** remains almost unchanged which demonstrates the good circulation stability of **1** in actual application. The above results indicate that **1** possesses good thermal/chemical stability, high separ-

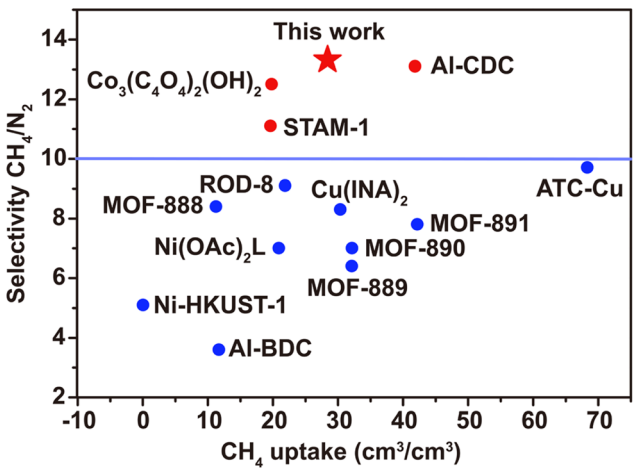

Fig. 5 Comparison of the IAST selectivity for a CH_4/N_2 mixture and CH_4 adsorption of **1** with those of previously reported CH_4-selective MOFs at 298 K and 1 bar. Red represents selectivity higher than 10, and blue represents selectivity lower than 10.

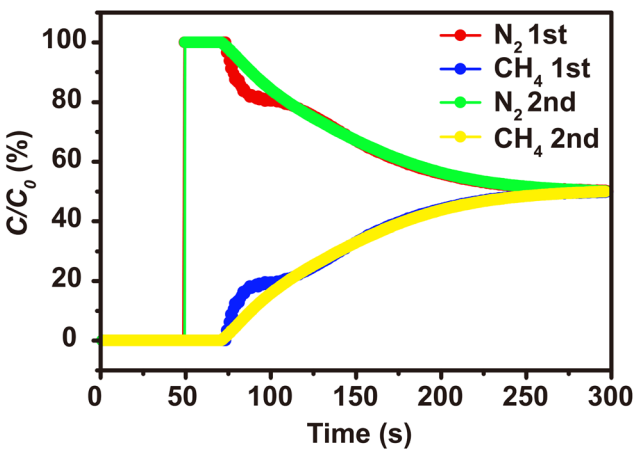

Fig. 7 Experimental breakthrough curves of N_2/CH_4 (v : v = 1 : 1) at 298 K during two consecutive cycles (red and blue for the 1st cycle; green and yellow for the 2nd cycle).

ation selectivity for CH_4/N_2 and good recyclability which make this MOF have potential application in CH_4 purification.

In conclusion, a pillar-layered multi-component metal–organic framework $[CuCeL(Cl4\text{-}bdc)_{0.5}(H_2O)_2\cdot(H_2O)_6]_n$ was constructed. Through the coordination bonds between Cl_4-bdc ligands and adjacent 3d–4f layers, 1D open channels along the *a*-axis and small confined cavities along the sides of channels were constructed precisely. Due to the synergistic effect between the abundant Cl atoms in Cl_4-bdc which can form multiple C–H···Cl interactions and the confinement effect which enhances the interaction between guest molecules and host framework, this MOF exhibits a strong binding effect for CH_4. More strikingly, this synergistic effect can enhance the CH_4 affinity and endow **1** with great separation ability for CH_4/N_2. As a result, **1** presents a high CH_4 adsorption capacity of 28.41 cm^3/cm^3 at 298 K and high IAST selectivity of 13.32 for CH_4/N_2 separation. DFT calculations show that the confined cavity which is decorated by chlorine atoms is crucial to binding CH_4 molecules and can be used as a molecular trap for CH_4. The breakthrough experiments revealed that the MOF-based CH_4 nano-trap is a new benchmark for CH_4/N_2 separation and this MOF can be a potential material for capturing CH_4 from coal-mine methane to recover fuel and reduce greenhouse gas emissions.

Conflicts of interest

There are no conflicts to declare.

Acknowledgements

This work was supported by the National Natural Science Foundation of China (21571139, 22035003, 22001132, 22271217).

References

1 Y. He, W. Zhou, G. Qian and B. Chen, Methane storage in metal-organic frameworks, *Chem. Soc. Rev.*, 2014, **43**, 5657–5678.
2 D. Saha, H. A. Grappe, A. Chakraborty and G. Orkoulas, Postextraction separation, on-board storage, and catalytic conversion of methane in natural gas: a review, *Chem. Rev.*, 2016, **116**, 11436–11499.
3 M. Chang, Y. Zhao, D. Liu, J. Yang, J. Li and C. Zhong, Methane-trapping metal–organic frameworks with an aliphatic ligand for efficient CH_4/N_2 separation, *Sustainable Energy Fuels*, 2020, **4**, 138–142.
4 S. M. Wang, M. Shivanna and Q. Y. Yang, Nickel-based metal-organic frameworks for coal-bed methane purification with record CH_4/N_2 selectivity, *Angew. Chem., Int. Ed.*, 2022, **61**, e202201017.
5 H. Wang, Y. Liu and J. Li, Designer metal-organic frameworks for size-exclusion-based hydrocarbon separations: progress and challenges, *Adv. Mater.*, 2020, **32**, 2002603.
6 J. Liu, H. Shang, J. Yang, J. Wang, J. Li and S. Deng, Novel zeolite/carbon monolith adsorbents for efficient CH_4/N_2 separation, *Chem. Eng. J.*, 2021, **426**, 130163.
7 R. Tang, Q. Dai, W. Liang, Y. Wu, X. Zhou, H. Pan and Z. Li, Synthesis of novel particle rice-based carbon materials and its excellent CH_4/N_2 adsorption selectivity for methane enrichment from Low-rank natural gas, *Chem. Eng. J.*, 2020, **384**, 123388.
8 Z. Yang, D. Wang, Z. Meng and Y. Li, Adsorption separation of CH_4/N_2 on modified coal-based carbon molecular sieve, *Sep. Purif. Technol.*, 2019, **218**, 130–137.
9 Y. Wu, D. Yuan, D. He, J. Xing, S. Zeng, S. Xu, Y. Xu and Z. Liu, Decorated traditional zeolites with subunits of metal-organic frameworks for CH_4 /N_2 separation, *Angew. Chem., Int. Ed.*, 2019, **58**, 10241–10244.
10 S. Xu, W. C. Li, C. T. Wang, L. Tang, G. P. Hao and A. H. Lu, Self-pillared ultramicroporous carbon nanoplates for selective separation of CH_4 /N_2, *Angew. Chem., Int. Ed.*, 2021, **60**, 6339–6343.
11 Q. Shi, J. Wang, H. Shang, H. Bai, Y. Zhao, J. Yang, J. Dong and J. Li, Effective CH_4 enrichment from N_2 by SIM-1 via a strong adsorption potential SOD cage, *Sep. Purif. Technol.*, 2020, **230**, 115850.
12 M. Chang, T. Yan, Y. Wei, J.-X. Wang, D. Liu and J.-F. Chen, Enhancing CH_4 capture from coalbed methane through tuning van der Waals affinity within isoreticular Al-based metal–organic frameworks, *ACS Appl. Mater. Interfaces*, 2022, **14**, 25374–25384.
13 Z. Niu, X. Cui, T. Pham, P. C. Lan, H. Xing, K. A. Forrest, L. Wojtas, B. Space and S. Ma, A metal-organic framework based methane nano-trap for the capture of coal-mine methane, *Angew. Chem., Int. Ed.*, 2019, **58**, 10138–10141.
14 C. E. Kivi, B. S. Gelfand, H. Dureckova, H. T. K. Ho, C. Ma, G. K. H. Shimizu, T. K. Woo and D. Song, 3D porous metal-organic framework for selective adsorption of methane over dinitrogen under ambient pressure, *Chem. Commun.*, 2018, **54**, 14104–14107.
15 D. Saha, G. Orkoulas, S. Yohannan, H. C. Ho, E. Cakmak, J. Chen and S. Ozcan, Nanoporous boron nitride as exceptionally thermally stable adsorbent: role in efficient separation of light hydrocarbons, *ACS Appl. Mater. Interfaces*, 2017, **9**, 14506–14517.
16 K. X. Yao, Y. Chen, Y. Lu, Y. Zhao and Y. Ding, Ultramicroporous carbon with extremely narrow pore distribution and very high nitrogen doping for efficient methane mixture gases upgrading, *Carbon*, 2017, **122**, 258–265.
17 X. Ren, T. Sun, J. Hu and S. Wang, Highly enhanced selectivity for the separation of CH_4 over N_2 on two ultra-microporous frameworks with multiple coordination modes, *Microporous Mesoporous Mater.*, 2014, **186**, 137–145.
18 P. T. K. Nguyen, H. T. D. Nguyen, H. Q. Pham, J. Kim, K. E. Cordova and H. Furukawa, Synthesis and selective CO_2 capture properties of a series of hexatopic linker-based

metal–organic frameworks, *Inorg. Chem.*, 2015, **54**, 10065–10072.

19 X. W. Liu, Y. Guo, A. Tao, M. Fischer, T. J. Sun, P. Z. Moghadam, D. Fairen-Jimenez and S. D. Wang, "Explosive" synthesis of metal-formate frameworks for methane capture: an experimental and computational study, *Chem. Commun.*, 2017, **53**, 11437–11440.

20 J. Hu, T. Sun, X. Liu, Y. Guo and S. Wang, Separation of CH_4/N_2 mixtures in metal–organic frameworks with 1D micro-channels, *RSC Adv.*, 2016, **6**, 64039–64046.

21 Y. Guo, J. Hu, X. Liu, T. Sun, S. Zhao and S. Wang, Scalable solvent-free preparation of $[Ni_3(HCOO)_6]$ frameworks for highly efficient separation of CH_4 from N_2, *Chem. Eng. J.*, 2017, **327**, 564–572.

22 A. Jayaraman, A. J. Hernandez-Maldonado, R. T. Yang, D. Chinn, C. L. Munson and D. H. Mohr, Clinoptilolites for nitrogen/methane separation, *Chem. Eng. Sci.*, 2004, **59**, 2407–2417.

23 D. Saha, Z. Bao, F. Jia and S. Deng, Adsorption of CO_2, CH_4, N_2O, and N_2 on MOF-5, MOF-177, and Zeolite 5A, *Environ. Sci. Technol.*, 2010, **44**, 1820–1826.

24 H. Noh, C.-W. Kung, T. Islamoglu, A. W. Peters, Y. Liao, P. Li, S. J. Garibay, X. Zhang, M. R. DeStefano, J. T. Hupp and O. K. Farha, Room temperature synthesis of an 8-connected Zr-based metal–organic framework for top-down nanoparticle encapsulation, *Chem. Mater.*, 2018, **30**, 2193–2197.

25 R.-B. Lin, S. Xiang, W. Zhou and B. Chen, Microporous metal-organic framework materials for gas separation, *Chem*, 2020, **6**, 337–363.

26 S. Wang, H. Reinsch, N. Heymans, M. Wahiduzzaman, C. Martineau-Corcos, G. De Weireld, G. Maurin and C. Serre, Toward a rational design of titanium metal-organic frameworks, *Matter*, 2020, **2**, 440–450.

27 M. Chang, J. Ren, Q. Yang and D. Liu, A robust calcium-based microporous metal-organic framework for efficient CH_4/N_2 separation, *Chem. Eng. J.*, 2021, **408**, 127294.

28 X. Jia, N. Yuan, L. Wang, J. Yang and J. Li, $(CH_3)_2NH$–assisted synthesis of high–purity Ni–HKUST–1 for the adsorption of CO_2, CH_4, and N_2, *Eur. J. Inorg. Chem.*, 2018, **8**, 1047–1052.

29 R. B. Lin, L. Li, H. L. Zhou, H. Wu, C. He, S. Li, R. Krishna, J. Li, W. Zhou and B. Chen, Molecular sieving of ethylene from ethane using a rigid metal-organic framework, *Nat. Mater.*, 2018, **17**, 1128–1133.

30 A. Cadiau, K. Adil, P. M. Bhatt, Y. Belmabkhout and M. Eddaoudi, A metal-organic framework-based splitter for separating propylene from propane, *Science*, 2016, **353**, 137–140.

31 H. Wang, X. Dong, V. Colombo, Q. Wang, Y. Liu, W. Liu, X. L. Wang, X. Y. Huang, D. M. Proserpio, A. Sironi, Y. Han and J. Li, Tailor-made microporous metal-organic frameworks for the full separation of propane from propylene through selective size exclusion, *Adv. Mater.*, 2018, **30**, 1805088.

32 B. Liang, X. Zhang, Y. Xie, R. B. Lin, R. Krishna, H. Cui, Z. Li, Y. Shi, H. Wu, W. Zhou and B. Chen, An ultramicroporous metal-organic framework for high sieving separation of propylene from propane, *J. Am. Chem. Soc.*, 2020, **142**, 17795–17801.

33 J. Wang, Y. Zhang, P. Zhang, J. Hu, R. Lin, Q. Deng, Z. Zeng, H. Xing, S. Deng and B. Chen, Optimizing pore space for flexible-robust metal-organic framework to boost trace acetylene removal, *J. Am. Chem. Soc.*, 2020, **142**, 9744–9751.

34 T. Ke, Q. Wang, J. Shen, J. Zhou, Z. Bao, Q. Yang and Q. Ren, Molecular sieving of C_2-C_3 alkene from alkyne with tuned threshold pressure in robust layered metal-organic frameworks, *Angew. Chem., Int. Ed.*, 2020, **59**, 12725–12730.

35 Y. T. Zhang, X. L. Wang, E. L. Zhou, X. S. Wu, B. Q. Song, K. Z. Shao and Z. M. Su, Polyoxovanadate-based organic-inorganic hybrids: from $\{V_5O_9Cl\}$ clusters to nanosized octahedral cages, *Dalton Trans.*, 2016, **45**, 3698–3701.

36 M. O'Keeffe, M. A. Peskov, S. J. Ramsden and O. M. Yaghi, The reticular chemistry structure resource (RCSR) database of, and symbols for, crystal nets, *Acc. Chem. Res.*, 2009, **41**, 1782–1789.

37 V. Robins, S. J. Ramsden and S. T. Hyde, 2D hyperbolic groups induce three-periodic euclidean reticulations, *Eur. Phys. J. B*, 2004, **39**, 365–375.

38 A. P. Shevchenko, I. A. Blatov, E. V. Kitaeva and V. A. Blatov, Local coordination versus overall topology in crystal structures: deriving knowledge from crystallographic databases, *Cryst. Growth Des.*, 2016, **17**, 774–785.

39 L.-H. Xie, X.-M. Liu, T. He and J.-R. Li, Metal-Organic Frameworks for the Capture of Trace Aromatic Volatile Organic Compounds, *Chem*, 2018, **4**, 1911–1927.

40 L. Li, L. Yang, J. Wang, Z. Zhang, Q. Yang, Y. Yang, Q. Ren and Z. Bao, Highly efficient separation of methane from nitrogen on a squarate-based metal-organic framework, *AIChE J.*, 2018, **64**, 3681–3689.

41 R.-J. Li, M. Li, X.-P. Zhou, S. W. Ng, M. O'Keeffe and D. Li, ROD-8, a rod MOF with a pyrene-cored tetracarboxylate linker: framework disorder, derived nets and selective gas adsorption, *CrystEngComm*, 2014, **16**, 6291–6295.